Draft version June 30, 2020
Typeset using LaTeX **twocolumn** style in AASTeX61

arXiv:2006.15150v1 [astro-ph.GA] 26 Jun 2020

POPULATING THE LOW-MASS END OF THE $M_{\rm BH} - \sigma_*$ RELATION

Vivienne F. Baldassare,[1,*] Claire Dickey,[1] Marla Geha,[1] and Amy E. Reines[2]

[1] *Yale University*
Department of Astronomy
52 Hillhouse Avenue
New Haven, CT 06511, USA
[2] *eXtreme Gravity Institute*
Department of Physics
Montana State University
Bozeman, MT 59717 USA

(Received 28 May 2020; Accepted 26 June 2020)

Submitted to ApJL

ABSTRACT

We present high resolution spectroscopy taken with the Keck Echellete Spectrograph and Imager to measure stellar velocity dispersions for eight active dwarf galaxies ($M_* < 3 \times 10^9\ M_\odot$) with virial black hole masses. We double the number of systems in this stellar mass regime with measurements of both black hole mass ($M_{\rm BH}$) and stellar velocity dispersion (σ_*), and place them on the $M_{\rm BH} - \sigma_*$ relation. The tight relation between $M_{\rm BH}$ and σ_* for higher mass galaxies is a strong piece of evidence for the co-evolution of BHs and their host galaxies, but it has been unclear whether this relation holds in the dwarf galaxy regime. Our sample is in good agreement with the extrapolation of the $M_{\rm BH} - \sigma_*$ relation to low BH/galaxy masses, suggesting that the processes which produce $M_{\rm BH} - \sigma_*$ can also operate in dwarf galaxies. These results provide important constraints for massive black hole seed formation models and models exploring the impact of AGN feedback in dwarf galaxies.

Corresponding author: Vivienne F. Baldassare
vivienne.baldassare@yale.edu

* Einstein Fellow

1. INTRODUCTION

Central massive black holes (BHs) exist in virtually all galaxies with stellar masses $M_* \gtrsim 10^{10}\ M_\odot$ (Magorrian et al. 1998). There are scaling relations between the mass of the central BH and properties of the host galaxy (Kormendy & Ho 2013), such as galaxy stellar mass (Reines & Volonteri 2015) , the mass/luminosity of the stellar bulge (Läsker et al. 2014; Schutte et al. 2019), and the velocity dispersion of stars in the bulge (Ferrarese & Merritt 2000; Gebhardt et al. 2000; Gültekin et al. 2009). These scaling relations are key to our understanding of how BH growth relates to the evolution of galaxies.

The most well studied of these scaling relations is between stellar velocity dispersion and BH mass, also known as the $M_{\rm BH} - \sigma_*$ relation. There is a large body of work exploring the $M_{\rm BH} - \sigma_*$ relation for relatively high-mass galaxies (e.g., Gültekin et al. 2009; Kormendy & Ho 2013; McConnell & Ma 2013; Woo et al. 2013; van den Bosch 2016; Krajnović et al. 2018), and its existence points towards feedback between the growth of the BH and its host galaxy.

The low-mass end of the $M_{\rm BH} - \sigma_*$ relation is of particular importance as it is predicted to give insight into the formation mechanisms of BH seeds at high redshift, as well as into the efficiency of BH growth in small galaxies (Greene et al. 2019). In particular, different BH seed formation mechanisms (i.e., Pop III stars versus direct collapse) may be reflected in the the slope and scatter of the low-mass end of $M_{\rm BH} - \sigma_*$ (Volonteri & Natarajan 2009). Lighter Pop III seeds are predicted to produce a present-day population of under-massive BHs, while heavier direct collapse seeds would result in a flattening of $M_{\rm BH} - \sigma_*$ around BH masses of $\sim 10^5\ M_\odot$. BH fueling may also impact where low-mass BHs/galaxies fall on the relation (Ricarte & Natarajan 2018). Pacucci et al. (2018) predicts that BH accretion should be bimodal, with BHs $\lesssim 10^5\ M_\odot$ accreting inefficiently, resulting in a population of low-mass BHs that fall beneath the present-day $M_{\rm BH} - \sigma_*$ relation.

Unfortunately, it has been difficult to probe $M_{\rm BH} - \sigma_*$ in the dwarf galaxy regime. In addition to the observational difficulty of detecting low-mass BHs (Reines & Comastri 2016; Baldassare et al. 2018, 2019; Reines et al. 2020), measuring σ_* in these systems requires high spectral resolution observations of faint galaxies. In the last several years, large-scale optical spectroscopic surveys have helped with the former; there has been a substantial increase in the number of known active galactic nuclei (AGN) in low-mass galaxies, which can now be used to probe scaling relations at the low-mass end (Reines et al. 2013; Moran et al. 2014; Baldassare et al. 2015; Sartori et al. 2015).

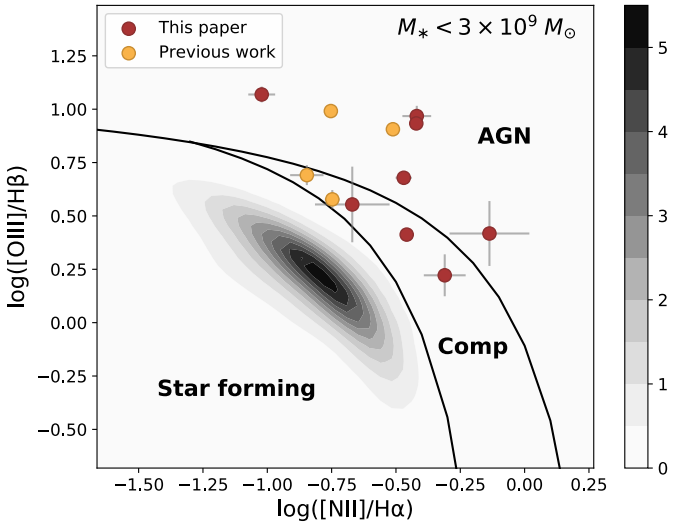


Figure 1. BPT diagram of the active dwarf galaxies we place on the $M_{\rm BH} - \sigma_*$ relation. The points include the 10 broad-line AGN from Reines et al. (2013), RGG 118, and Pox 52. Galaxies for which we have obtained new velocity dispersion measurements are shown as red circles; objects with existing measurements are shown in orange. The shaded contours show the positions of galaxies with $M_* < 3 \times 10^9\ M_\odot$ from the NASA-Sloan Atlas (30654 galaxies). Line flux measurements for the active dwarf galaxies are from Reines et al. (2013); fluxes for the other systems are from the NASA-Sloan Atlas.

Motivated by the power of scaling relations for exploring BH formation and fueling, we obtained new stellar velocity dispersion measurements for eight dwarf galaxies ($M_* < 3 \times 10^9\ M_*$) with low-mass BHs and explore the low-mass end of $M_{\rm BH} - \sigma_*$. With our observations, we double the number of dwarf galaxies on $M_{\rm BH} - \sigma_*$. Section 2 describes our sample and observations; Section 3 discusses our velocity dispersion and BH mass measurements; Section 4 presents the $M_{\rm BH} - \sigma_*$ relation including our low-mass systems and discusses implications.

2. SAMPLE AND OBSERVATIONS

In this work, we measure stellar velocity dispersions for eight nearby ($z < 0.055$) active dwarf galaxies with optical spectroscopic signatures of AGN activity. These systems are drawn from the sample of Reines et al. (2013) dwarf galaxies with both broad and narrow optical emission line signatures of AGN activity (using the BPT diagram; Baldwin et al. 1981; Kewley et al. 2006). They were originally selected from the NASA-Sloan At-

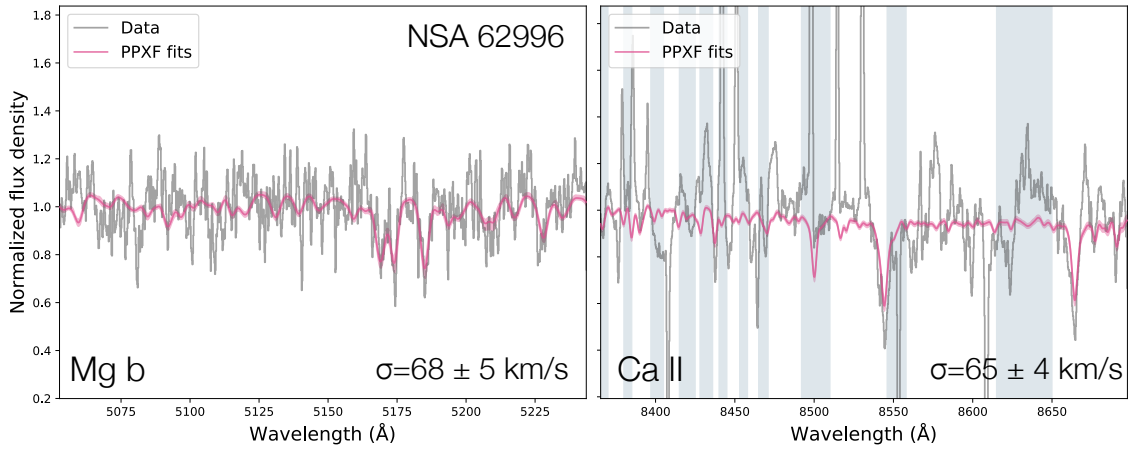


Figure 2. ESI spectrum and pPXF fits for NSA 62996. In each panel, the data is shown in gray and the best-fit pPXF models are shown in pink. The solid pink line is the mean pPXF fit, and the shaded pink region encompasses all 1000 fits. The left panel shows the region surrounding the Mg Ib triplet, and the right panel shows the region surrounding the Ca II triplet. The locations of sky lines are masked in fitting and marked by shaded blue regions in the figure. The velocity dispersion and uncertainties are given in the bottom right of each panel. Spectrum is smoothed with a box size of 3 pixels for plotting. Additional spectra shown in Figures 5 and 6.

las[1], a catalog of local galaxies with SDSS imaging and spectroscopy and derived quantities such as stellar mass. Reines et al. (2013) identified 10 systems meeting the above criteria; two of these have velocity dispersions measured in previous works. The observations presented here complete the velocity dispersion measurements for all of the Reines et al. (2013) active dwarf galaxies with BH mass estimates. Figure 1 shows where the active dwarf galaxy sample falls on the BPT diagram. Stellar masses range from $8 \times 10^8 - 3 \times 10^9\ M_\odot$.

In addition to the eight new systems presented here, we include seven dwarf galaxies with velocity dispersions and BH masses measured in the literature. These include NGC 4395 (Filippenko & Sargent 1989; Filippenko & Ho 2003), Pox 52 (Barth et al. 2004; Thornton et al. 2008), RGG 118 (Baldassare et al. 2015, 2017a), RGG 119 (Baldassare et al. 2016), M 32 (van den Bosch & de Zeeuw 2010), and NGC 5206 and NGC 205 (Nguyen et al. 2018, 2019).

Observations were taken with the Keck II Echellette Spectrograph and Imager (ESI; Sheinis et al. 2002) on 10 March 2018 and 4 September 2019. Observations were made with the 0.75″ x 20″ slit, which gives an instrumental resolution of 23 km s^{-1} across the wavelength range 3900-11000 Å. The dispersion ranges from 0.16Å/pixel in the blue to 0.30Å/pixel in the red, giving a constant velocity dispersion of 11.5 km s^{-1} pixel^{-1}. Total exposure times ranged from 1200-2700 seconds, and were split into three exposures to facilitate cosmic ray removal. The per-pixel signal-to-noise ratios of the spectra range from $\sim 3 - 20$, with a median signal-to-noise ratio of 8.

We used `XIDL`[2] (Prochaska et al. 2003) for the initial reduction of the science frames. Separate wavelength solutions were derived for each night of observations from a combination of CuAr and HgNe+Xe arcs. Cosmic rays were removed from each frame with `LACosmic` (van Dokkum 2001). Individual exposures were then median combined and rectified so that the spatial scale of the pixels are the same across all orders. The background sky was modelled with a bspline fit to the outer 2″ on each side of the slit.

1-D spectra were optimally extracted (Horne 1986) using a width of 6 pixels, which corresponds to an extraction width of $\sim 1''$. At the distances of our sample, this corresponds to $0.5 - 1$ kpc.

3. ANALYSIS

3.1. *Velocity dispersions*

We use the Penalized Pixel Fitting software (pPXF; Cappellari & Emsellem 2004; Cappellari 2017) to measure stellar velocity dispersions. pPXF fits the absorption line spectra of galaxies using a library of stellar spectra and extracts galaxy stellar kinematics. We use a library of 9 stars ranging in spectral type from F to M. They were observed with ESI using the same slit width as the galaxy observations. The best fits include a combination of several stellar spectra. We fit the kine-

[1] nsatlas.org

[2] https://www2.keck.hawaii.edu/inst/esi/ESIRedux/index.html

matics in two regions: one surrounding the Mg Ib triplet at $\sim 5160 - 5190$Å and another surrounding the Ca II triplet at $\sim 8490 - 8670$Å. The uncertainty in the velocity dispersion is computed with a Monte Carlo bootstrap method (Geha et al. 2009). We add noise to the 1-D spectrum, then recalculate the velocity dispersion for 1000 noise realizations. The final value is taken to be the mean recovered velocity dispersion, and the uncertainty is taken to be the square root of the variance relative to the mean.

At the redshifts of our sample, the Ca II triplet falls at the end of the ESI spectrum in a region with substantial contamination from sky lines. While we measure Mg Ib velocity dispersions for all eight objects, it is only possible to obtain Ca II measurements for four. When we can fit both regions, the estimates are consistent with one another and we adopt the mean as the final velocity dispersion measurement. For the rest, we adopt the Mg Ib measurements. Figure 2 shows the ESI spectra and pPXF fits to the Mg Ib and Ca II regions for NSA 62996. Table 1 gives the velocity dispersion measurements for the systems analyzed here along with measurements for seven dwarf galaxies reported in previous works.

The values reported in Table 1 correspond to those measured in the $1''$ extracted spectrum. This is well-matched to the bulge properties found for this sample by Schutte et al. (2019) using HST observations; their median bulge diameter is 0.6 kpc. Here, the term "bulge" is used to refer to the inner Sérsic component, though most have Sérsic indices that are below that of a classical bulge. We also measure the stellar kinematics in spectra extracted between 0.5 and $1.5''$ on either side of the central arcsecond; we find that these values are consistent with flat velocity dispersion profiles. This is in good agreement with the velocity dispersion profiles measured for more nearby dwarf elliptical galaxies (Geha et al. 2006, 2010; Toloba et al. 2014).

3.2. *Black hole masses*

BH masses for the eight systems analyzed in this work are taken from Reines & Volonteri (2015). The BH masses are single-epoch spectroscopic masses computed using the broad Hα emission line. Under the assumption that gas in the broad line emitting region is virialized, one can estimate the BH mass as $M_{\rm BH} = f\frac{v^2 R_{\rm BLR}}{G}$, where v is the characteristic velocity of gas in the broad line region, $R_{\rm BLR}$ is the distance to the broad line region, and f is a factor intended to take into account the unknown broad line region geometry. The full-width half maximum of the broad Hα line is used to estimate the characteristic velocity, and the luminosity of broad Hα is a proxy for the distance to the broad line region (Greene & Ho 2005; Bentz et al. 2009, 2013). BH masses estimated using this technique have systematic uncertainties of ~ 0.4 dex. We do not recompute BH masses using the ESI data, but do confirm that the broad Hα line widths are consistent between the SDSS and ESI data.

4. THE $M_{\rm BH} - \sigma_*$ RELATION WITH DWARF GALAXIES

Figure 3 shows the locations of the eight active dwarf galaxies analyzed here on the $M_{\rm BH} - \sigma_*$ relation, as well as the positions of the seven dwarf galaxies from the literature. We also include the sample of low-mass AGN ($M_{\rm BH} \lesssim 2 \times 10^6\ M_\odot$) with measured stellar velocity dispersions from Xiao et al. (2011) and galaxies with dynamical BH mass measurements from the Kormendy & Ho (2013) compilation. Most of the dwarf galaxies in the active sample are in good agreement with both the the $M_{\rm BH} - \sigma_*$ relation found by Kormendy & Ho (2013) using dynamical BH masses, and the relation found by Xiao et al. (2011) for broad-line AGNs in the Greene & Ho (2007) sample.

It is interesting to consider galaxy-scale properties which may influence BH growth and thus result in a galaxy falling above or below the $M_{\rm BH} - \sigma_*$ relation. In Figure 4 we plot the deviation from the Kormendy & Ho (2013) relation versus galaxy properties to search for properties which may impact BH growth and produce over/under-massive BHs relative to $M_{\rm BH} - \sigma_*$. We consider the BH mass-to-stellar mass ratio, Eddington fraction, inner Sérsic index, and g-r color. Stellar masses are taken from Reines & Volonteri (2015). Eddington fractions are computed using X-ray luminosities reported in Dong et al. (2012) and Baldassare et al. (2017b) and a bolometric correction of 10 (Marconi & Hunt 2003). The bulge Sérsic indexes were determined using *Hubble Space Telescope* imaging by Jiang et al. (2011) and Schutte et al. (2019). The (g-r) color is computed using the NASA-Sloan Atlas Galactic-extinction corrected fluxes.

According to Spearman rank correlation coefficients, we find no significant correlations between the above properties and the deviation from the $M_{\rm BH} - \sigma_*$ relation, though we are limited by a relatively small sample size. The median ratio of BH to galaxy stellar mass is $\sim 10^{-4}$, roughly an order of magnitude lower than more massive elliptical galaxies (Reines & Volonteri 2015). The lack of a correlation between $M_{\rm BH} - \sigma_*$ deviation and Eddington fraction suggests that the current Eddington fraction does not reflect sustained BH growth over a long period of time. Similarly, the lack of correlation between bulge Sérsic index and $M_{\rm BH} - \sigma_*$ deviation suggests BH

Table 1. Dwarf galaxies with stellar velocity dispersions and black hole masses

Name	R13 ID	Redshift	Morphology	$\log_{10}(M_*/M_\odot)$	$\log_{10}(M_{\rm BH}/M_\odot)$	σ_* [km/s]	Reference
NSA 62996	1	0.0459	S0	9.45	5.80	66 ± 3	This paper
NSA 10779	9	0.0466	dE	9.30	5.44	34 ± 6 [a]	This paper
NSA 125318	11	0.0327	S0	9.24	5.00	41 ± 6	This paper
NSA 52675	20	0.0144	S0	9.29	6.10	53 ± 5	This paper
NSA 15235	32	0.0299	Spiral	9.30	5.29	42 ± 14 [a]	This paper
NSA 47066	48	0.0410	Spiral	9.12	5.42	32 ± 5 [a]	This paper
NSA 18913	123	0.0395	Disk	8.96	5.18	33 ± 14 [a]	This paper
NSA 99052	127	0.0317	Disk	9.36	5.21	52 ± 5	This paper
NGC 4395	21	0.0011	Spiral	9.10	5.0	< 30	Filippenko & Ho (2003)
NSA 166155	118	0.0243	Spiral	9.34	4.7	28 ± 11	Baldassare et al. (2015)
NSA 79874	119	0.0384	S0	9.36	5.46	28 ± 7	Baldassare et al. (2016)
Pox 52	N/A	0.022	dE	9.08	5.2	36 ± 5	Barth et al. (2004)
NGC 205	N/A	-0.0008	dE	8.99	3.8[b]	40 ± 5	Nguyen et al. (2018, 2019)
NGC 5206	N/A	0.002	dE	9.38	5.8[b]	35 ± 1	Nguyen et al. (2018, 2019)
M 32	N/A	-0.0007	dE	9.0	6.4[b]	77 ± 3	van den Bosch & de Zeeuw (2010)

NOTE—Black hole masses and velocity dispersion measurements. [a] indicates that the velocity dispersion measurement uses Mg Ib only. [b] indicates a dynamical BH detection and mass estimate. Galaxy stellar masses and BH masses for objects in the Reines et al. (2013) sample are taken from Reines & Volonteri (2015). Morphologies are taken from Schutte et al. (2019) and the NASA/IPAC Extragalactic Database.

growth in dwarf galaxies is not necessarily related to the assembly of a bulge. The lack of correlation between galaxy color and $M_{\rm BH} - \sigma_*$ offset could reflect no difference in galaxy stellar populations; a more careful analysis involving a decomposition of galaxy light profiles and removal of the AGN contribution is necessary to fully explore this.

There are several recent theoretical works which suggest that the growth of lower-mass BH seeds may be inefficient (e.g., Habouzit et al. 2016; Anglés-Alcázar et al. 2017), and that this should be reflected in the $M_{\rm BH} - \sigma_*$ relation. Pacucci et al. (2018) use a semi-analytical model to track the growth of BH seeds and predict the present-day low-mass end of the $M_{\rm BH} - \sigma_*$ relation. Their model includes high and low-mass BH seeds formed via direct collapse and Pop III models, respectively. They find that, in general, systems deviate from $M_{\rm BH} - \sigma_*$ at low BH masses. This is because high mass BH seeds ($\gtrsim 10^5\ M_\odot$) can more easily accrete in a "high-efficiency regime"- a region in the 2-D parameter space of BH mass and gas number density that corresponds to sustained super-Eddington accretion (Pacucci et al. 2017). On the other hand, low-mass seeds almost never accrete in the high-efficiency regime. By present day, Pacucci et al. (2018) predict that the $M_{\rm BH} - \sigma_*$ relation should become steeper at low BH masses, with observational biases producing any observed flattening. They predict this down-turn should occur at $\sigma_* \approx 65 {\rm km\ s^{-1}}$.

The above implies that we find systems which fall on $M_{\rm BH} - \sigma_*$ because those are the BHs that are possible to find, while a population of under-massive BHs remains hidden. Our results – a population of low-mass systems which largely agree with $M_{\rm BH} - \sigma_*$, as well as some which scatter below it – are consistent with such a scenario. Finding BHs with masses $\lesssim 10^5\ M_\odot$ and which fall below $M_{\rm BH} - \sigma_*$ also disfavors models which include only heavy BH seeds formed via direct collapse (i.e., those that predict BH seeds which form with $M_{\rm BH} = 10^5\ M_\odot$). It is also important to note that the SDSS spectroscopy is only sensitive enough to detect broad Hα emission from a $\sim 10^4 M_\odot$ BH accreting at its Eddington ratio (Reines et al. 2013), so we are only sensitive to the most massive BHs in dwarf galaxies.

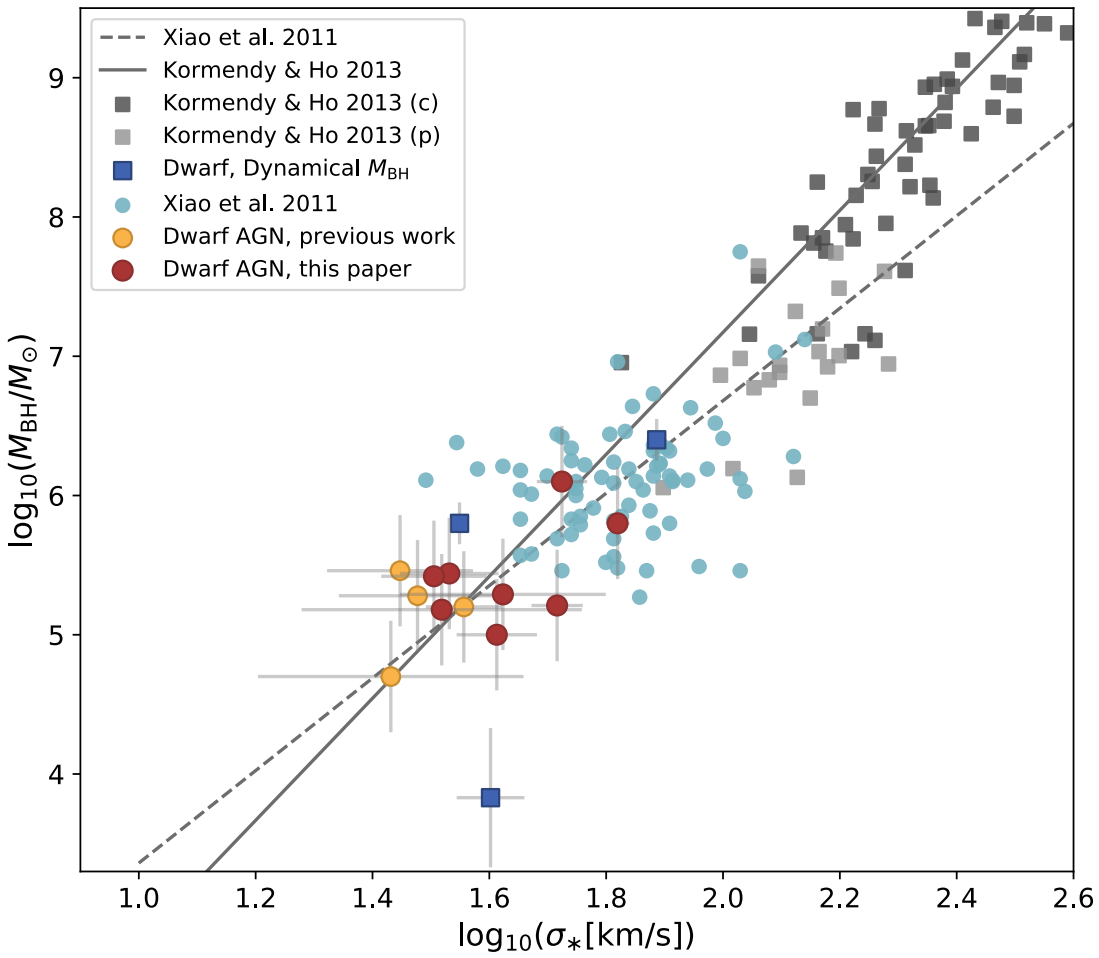


Figure 3. Black hole mass versus stellar velocity dispersion. The gray squares are from the compilation of Kormendy & Ho (2013); dark gray squares show galaxies with classical bulges and light gray squares show galaxies with pseudo-bulges. Light blue circles show data for low-mass AGNs from Xiao et al. (2011). Active dwarf galaxies with ESI stellar velocity dispersion measurements measured here are shown as red circles; active dwarf galaxies with existing data are shown in orange. Dwarf galaxies with dynamical BH mass estimates are shown as dark blue squares. We also show the fits to $M_{\rm BH} - \sigma_*$ from Xiao et al. (2011) (dashed line) and Kormendy & Ho (2013) (solid line).

Our results also have interesting implications for AGN feedback in dwarf galaxies. While dwarf galaxies are predominantly influenced by environment-triggered feedback (Geha et al. 2012), recent observational studies have found tantalizing evidence for AGN-driven quenching in dwarf galaxies (Penny et al. 2018; Dickey et al. 2019). This is supported by recent simulations; Sharma et al. (2019) study AGN feedback in dwarf galaxies in Romulus25 and find that BHs can quench galaxies of similar mass to those considered in this work. However, the exact mechanisms by which BHs influence dwarf galaxies remains uncertain, with some zoom-in simulations finding that AGN struggle to regulate global star formation rates (Koudmani et al. 2019).

Increasing the sample of dwarf galaxies on the $\rm M_{BH} - \sigma_*$ relation is critical for understanding the frequency and extent to which BHs influence galaxy evolution at low stellar masses. Our new sample of dwarf galaxies does not produce excessive scatter from the relation, suggesting that BH-galaxy co-evolution is still occurring at $\rm M_* \sim 10^9\ M_\odot$. In high-mass galaxies, analysis of the stellar populations of galaxies with over- and under-massive black holes has been used to argue for AGN feedback directly influencing star formation histories (e.g., Martín-Navarro & Mezcua 2018). Searching for similar trends between galaxy properties and position on the $\rm M_{BH} - \sigma_*$ relation will further inform our picture of AGN feedback in low mass galaxies. Further quantifying the scatter in the relationship is also key, as Silk (2017) suggests that dwarf galaxies following $M_{\rm BH} - \sigma_*$ while falling below the $M_{\rm BH} - M_*$ relation could be evidence for AGN-driven suppression of star

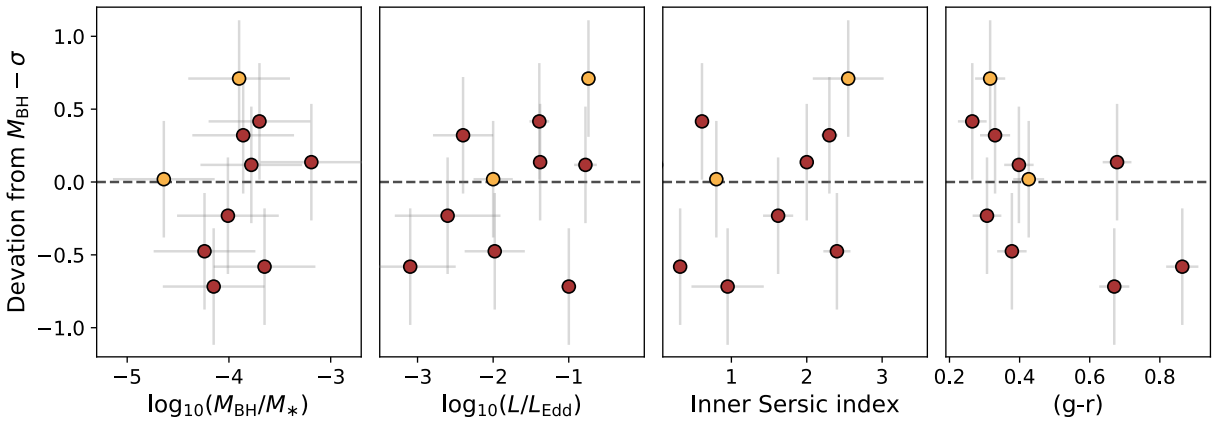


Figure 4. Deviation from $M_{\rm BH} - \sigma_*$ relation as a function of galaxy/BH properties. Color-coding is the same as in Figures 1 and 3. Deviation from $M_{\rm BH} - \sigma_*$ is defined as $\log_{10}(M_{\rm BH,measured}/M_{\rm BH,expected})$, where $M_{\rm BH,expected}$ is the BH mass predicted from the Kormendy & Ho (2013) $M_{\rm BH} - \sigma_*$ relation. From left to right, the deviation is plotted against the BH mass-to-stellar mass ratio, Eddington fraction, Sérsic index of the inner component, and dynamical mass-to-light ratio.

formation.

In summary, we have measured stellar velocity dispersions for eight active dwarf galaxies, doubling the number of dwarf galaxies on the $M_{\rm BH} - \sigma_*$ relation. These galaxies have BHs with masses ranging from $10^5 - 10^6\ M_\odot$. We find that these systems are in good agreement with the extrapolation of the $M_{\rm BH} - \sigma_*$ relation, implying that the processes which lead to the present-day $M_{\rm BH} - \sigma_*$ relation also apply to dwarf galaxies. This provides important constraints for models of BH formation and growth. Larger samples of dwarf galaxies with measured stellar velocity dispersions and BH masses are necessary to determine which properties impact BH growth in these systems.

Facility: Keck:II (ESI)

The authors thank the anonymous referee for their comments and suggestions which have improved this manuscript. Support for VFB was provided by the National Aeronautics and Space Administration through Einstein Postdoctoral Fellowship Award Number PF7-180161 issued by the Chandra X-ray Observatory Center, which is operated by the Smithsonian Astrophysical Observatory for and on behalf of the National Aeronautics Space Administration under contract NAS8-03060.

The data presented herein were obtained at the W. M. Keck Observatory, which is operated as a scientific partnership among the California Institute of Technology, the University of California and the National Aeronautics and Space Administration. The Observatory was made possible by the generous financial support of the W. M. Keck Foundation. The authors wish to recognize and acknowledge the very significant cultural role and reverence that the summit of Maunakea has always had within the indigenous Hawaiian community. We are most fortunate to have the opportunity to conduct observations from this mountain.

This research has made use of the NASA/IPAC Extragalactic Database (NED) which is operated by the Jet Propulsion Laboratory, California Institute of Technology, under contract with the National Aeronautics and Space Administration.

REFERENCES

Anglés-Alcázar, D., Faucher-Giguère, C.-A., Quataert, E., et al. 2017, MNRAS, 472, L109

Baldassare, V. F., Geha, M., & Greene, J. 2018, ApJ, 868, 152

—. 2019, arXiv e-prints, arXiv:1910.06342

Baldassare, V. F., Reines, A. E., Gallo, E., & Greene, J. E. 2015, ApJL, 809, L14

—. 2017a, ApJ, 850, 196

—. 2017b, ApJ, 836, 20

Baldassare, V. F., Reines, A. E., Gallo, E., et al. 2016, ApJ, 829, 57

Baldwin, J. A., Phillips, M. M., & Terlevich, R. 1981, PASP, 93, 5

Barth, A. J., Ho, L. C., Rutledge, R. E., & Sargent, W. L. W. 2004, ApJ, 607, 90

Bentz, M. C., Walsh, J. L., Barth, A. J., et al. 2009, ApJ, 705, 199

Bentz, M. C., Denney, K. D., Grier, C. J., et al. 2013, ApJ, 767, 149
Cappellari, M. 2017, MNRAS, 466, 798
Cappellari, M., & Emsellem, E. 2004, PASP, 116, 138
Dickey, C. M., Geha, M., Wetzel, A., & El-Badry, K. 2019, ApJ, 884, 180
Dong, R., Greene, J. E., & Ho, L. C. 2012, ApJ, 761, 73
Ferrarese, L., & Merritt, D. 2000, ApJL, 539, L9
Filippenko, A. V., & Ho, L. C. 2003, ApJL, 588, L13
Filippenko, A. V., & Sargent, W. L. W. 1989, ApJL, 342, L11
Gebhardt, K., Bender, R., Bower, G., et al. 2000, ApJL, 539, L13
Geha, M., Blanton, M. R., Yan, R., & Tinker, J. L. 2012, ApJ, 757, 85
Geha, M., Guhathakurta, P., Rich, R. M., & Cooper, M. C. 2006, AJ, 131, 332
Geha, M., van der Marel, R. P., Guhathakurta, P., et al. 2010, ApJ, 711, 361
Geha, M., Willman, B., Simon, J. D., et al. 2009, ApJ, 692, 1464
Greene, J. E., & Ho, L. C. 2005, ApJ, 630, 122
—. 2007, ApJ, 667, 131
Greene, J. E., Strader, J., & Ho, L. C. 2019, arXiv e-prints, arXiv:1911.09678
Gültekin, K., Richstone, D. O., Gebhardt, K., et al. 2009, ApJ, 698, 198
Habouzit, M., Volonteri, M., & Dubois, Y. 2016, ArXiv e-prints
Horne, K. 1986, PASP, 98, 609
Jiang, Y.-F., Greene, J. E., Ho, L. C., Xiao, T., & Barth, A. J. 2011, ApJ, 742, 68
Kewley, L. J., Groves, B., Kauffmann, G., & Heckman, T. 2006, MNRAS, 372, 961
Kormendy, J., & Ho, L. C. 2013, ARA&A, 51, 511
Koudmani, S., Sijacki, D., Bourne, M. A., & Smith, M. C. 2019, MNRAS, 484, 2047
Krajnović, D., Cappellari, M., McDermid, R. M., et al. 2018, MNRAS, 477, 3030
Läsker, R., Ferrarese, L., van de Ven, G., & Shankar, F. 2014, ApJ, 780, 70
Magorrian, J., Tremaine, S., Richstone, D., et al. 1998, AJ, 115, 2285
Marconi, A., & Hunt, L. K. 2003, ApJL, 589, L21
Martín-Navarro, I., & Mezcua, M. 2018, ApJL, 855, L20
McConnell, N. J., & Ma, C.-P. 2013, ApJ, 764, 184
Moran, E. C., Shahinyan, K., Sugarman, H. R., Vélez, D. O., & Eracleous, M. 2014, AJ, 148, 136
Nguyen, D. D., Seth, A. C., Neumayer, N., et al. 2018, ApJ, 858, 118
—. 2019, ApJ, 872, 104
Pacucci, F., Loeb, A., Mezcua, M., & Martín-Navarro, I. 2018, ApJL, 864, L6
Pacucci, F., Natarajan, P., Volonteri, M., Cappelluti, N., & Urry, C. M. 2017, ApJL, 850, L42
Penny, S. J., Masters, K. L., Smethurst, R., et al. 2018, MNRAS, 476, 979
Prochaska, J. X., Gawiser, E., Wolfe, A. M., Cooke, J., & Gelino, D. 2003, The Astrophysical Journal Supplement Series, 147, 227
Reines, A. E., & Comastri, A. 2016, PASA, 33, e054
Reines, A. E., Condon, J. J., Darling, J., & Greene, J. E. 2020, ApJ, 888, 36
Reines, A. E., Greene, J. E., & Geha, M. 2013, ApJ, 775, 116
Reines, A. E., & Volonteri, M. 2015, ApJ, 813, 82
Ricarte, A., & Natarajan, P. 2018, MNRAS, 481, 3278
Sartori, L. F., Schawinski, K., Treister, E., et al. 2015, MNRAS, 454, 3722
Schutte, Z., Reines, A. E., & Greene, J. E. 2019, ApJ, 887, 245
Sharma, R., Brooks, A., Somerville, R. S., et al. 2019, arXiv e-prints, arXiv:1912.06646
Sheinis, A. I., Bolte, M., Epps, H. W., et al. 2002, PASP, 114, 851
Silk, J. 2017, ApJL, 839, L13
Thornton, C. E., Barth, A. J., Ho, L. C., Rutledge, R. E., & Greene, J. E. 2008, ApJ, 686, 892
Toloba, E., Guhathakurta, P., Peletier, R. F., et al. 2014, ApJS, 215, 17
van den Bosch, R. C. E. 2016, ApJ, 831, 134
van den Bosch, R. C. E., & de Zeeuw, P. T. 2010, MNRAS, 401, 1770
van Dokkum, P. G. 2001, Publications of the Astronomical Society of the Pacific, 113, 1420
Volonteri, M., & Natarajan, P. 2009, MNRAS, 400, 1911
Woo, J.-H., Schulze, A., Park, D., et al. 2013, ApJ, 772, 49
Xiao, T., Barth, A. J., Greene, J. E., et al. 2011, ApJ, 739, 28

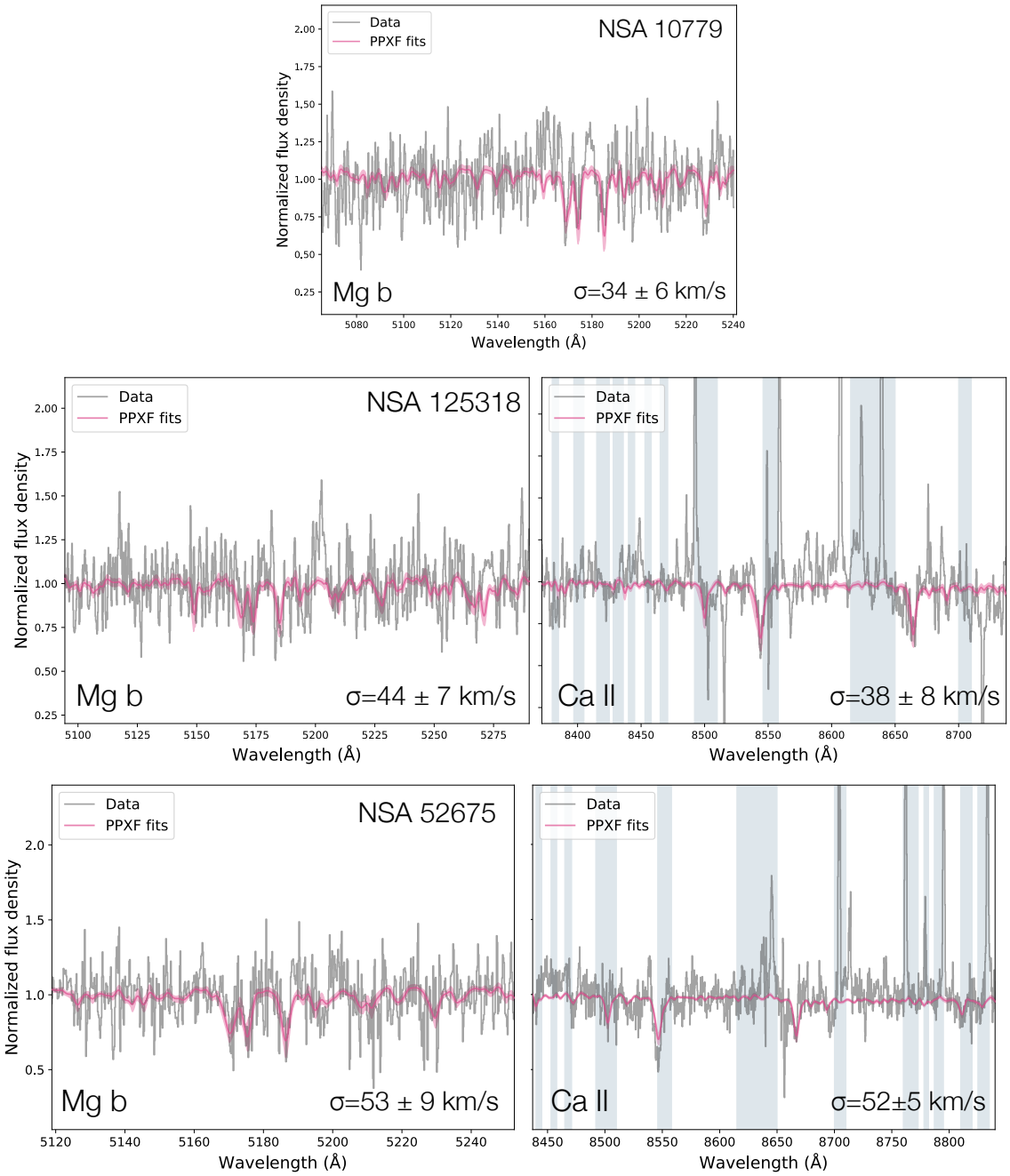


Figure 5. Same as Figure 2, but for additional objects. Spectra are smoothed with a box size of 3 pixels for plotting.

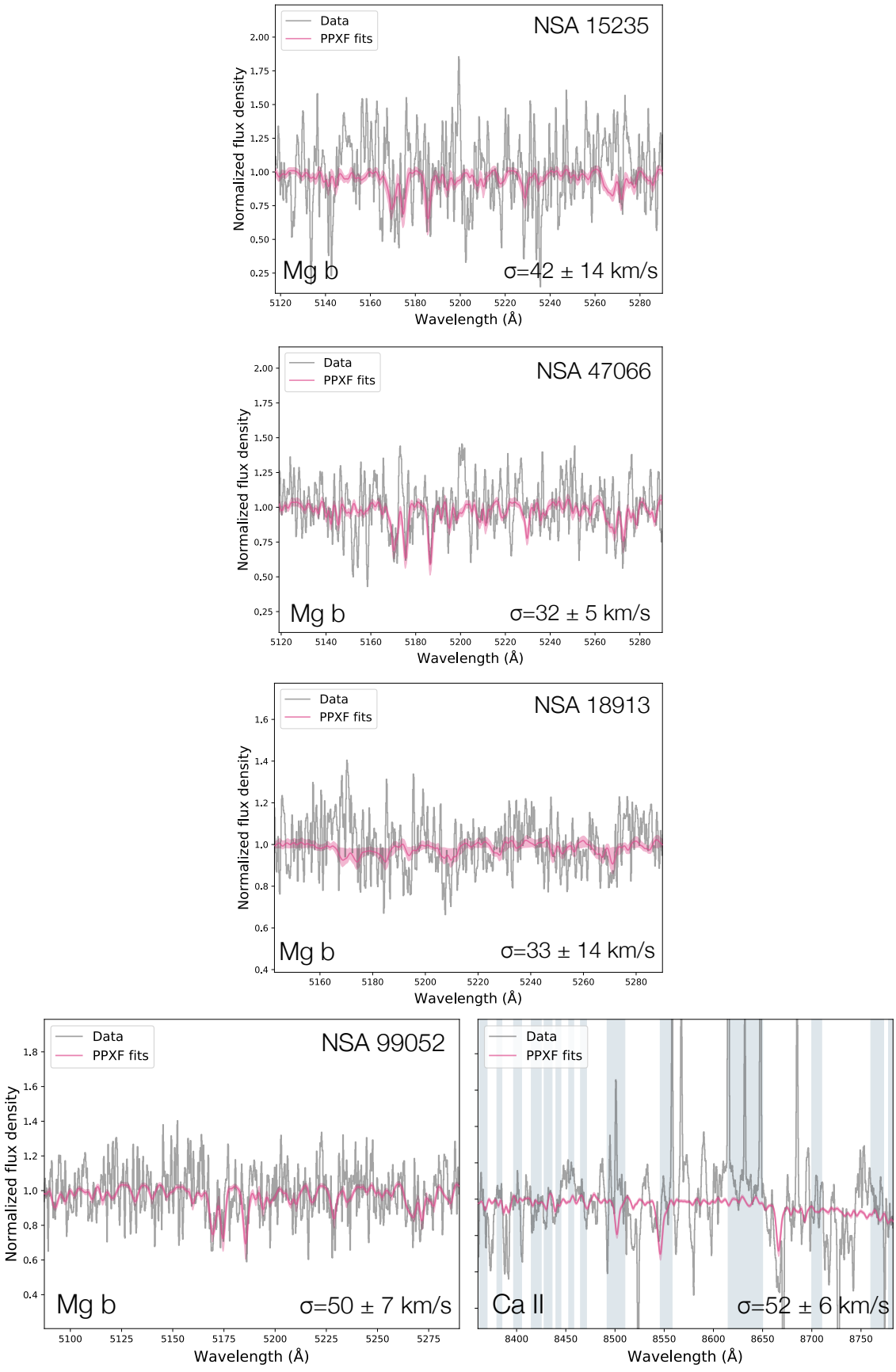


Figure 6. Same as Figure 2, but for additional objects. Spectra are smoothed with a box size of 3 pixels for plotting.